Oral Presentation

The 7th TSME International Conference on Mechanical Engineering
13-16 December 2016

TSME ICOME 2016
Mechanical Engineering Innovation for Green Society

AMM0009

Piezoelectrically-induced snap-through buckling in a buckled beam bonded with a segmented actuator

K. Tichakorn[1] , S. Aimmanee[1,*], K. Ruangjirakit[1]

[1]Advanced Materials and Structures Laboratory (AMASS), Department of Mechanical Engineering, King Mongkut's University of Technology Thonburi (KMUTT), 126 Pracha Uthit Rd., Bang Mod, Thung Khru, Bangkok 10140, Thailand

[*] Corresponding Author: sontipee@gmail.com

Abstract

In this paper, mathematical models are developed in order to analyze piezoelectrically-induced snap-through behaviors of bistable smart beams with different geometric configurations. The model delineates a beam bonded with a segmented piezoelectric material in the initial flat configuration. The smart beam is buckled into two stable shapes by edge shortening compression. A sudden change in transverse deflection during snap-through action of the buckled beam is stimulated by an extension of piezoelectric patch under electrical activation. The minimum potential energy principle associated with the Ritz and Lagrange multiplier method is utilized to predict shapes of the smart beam and the snapping-through critical voltage. Bordered Hessian is calculated to determine the stability of the shapes obtained. Size of the piezoelectric actuator is varied to search for the minimum critical electrical field. Experiments and finite element analyses are conducted to corroborate the computational results obtained from the model of the simply-supported smart beam. Comparisons among the different approaches reveal very good agreement in both mid-span displacements and snap-through voltages. Interestingly the lowest critical electrical field occurs when the piezoelectric patch covers around fifty to sixty percent of the beam platform area for both simply and clamped supported configurations. This model can give a very useful perspective in design of compliant structures with voltage control such as micro-switches, MEMS and other bistable beam mechanisms.

Keywords: bistable compliant mechanisms, piezoelectric material, smart beam, snap-through buckling

1. Introduction

Compliant mechanisms are mechanisms that consist of one or several flexible structural members. Through elastic body deformation, these members are utilized to transfer an input force or displacement. They have advantages over rigid-body or classical mechanisms for less relative moving parts, lower wear rate, lower cost, and better energy performance.

One example of compliant mechanisms is bistable buckled beams, which are commonly constructed in miniaturized technology such as micro-switches. This structure can transform between its two states of stable positions with some degree of disturbance tolerance. The action of shape changing between the two stable states are called snap-through buckling, which is a dynamic event. A snap-through buckling can generally be triggered by a sufficient amount of transverse force or bending moment. The resulting movement between the two stable positions provides a large induced displacement with relatively low magnitude of mechanical actuation.

Studies of bistable buckled beams have been mostly done by performing mathematical analysis to determine the critical lateral loads that trigger a snap-through buckling. The work of Cazottes et al (2009) [1] presented a model of a beam under the assumption of inextensible clamped condition. Numerical analysis was conducted along with the experiments to obtain the lateral force versus displacement diagram. The extensible beams assumption on the reduced elastica method were utilized by Camescasse et al. (2013) [2] to analyze simple buckled beams and their stability. The validated experiments performed by the same group were done later in 2014 [3]. Theses investigations provide conceptual guidelines for predicting the transverse load that activates snap-through buckling in different configurations. However, for applications in a limited enclosed space, using a smart material to induce snap-through action rather than applying a direct mechanical load is a better choice for engineering design. A beam bonded or embedded with a smart material i.e. piezoelectric material is dubbed as smart beam.

Deformation and motion of a bistable smart beam can be induced by elongation or contraction in the piezoelectric material under the application of electrical field. The configuration change between the stable states in this way is triggered by piezoelectricity, thus so-called piezoelectrically-induced snap-through buckling. Analogous to the critical force, research in bistable smart beam was focused on the critical voltage to trigger snap-through buckling (or snap-through voltage) and stability of corresponding deformed shapes. Maurini et al (2007) [4] considered a simple buckled beam with four piezoelectric actuators, where each two were attached on top and bottom surfaces of the beam substrate. The actuators on those surfaces filled the beam in full length. The extensible elastica method was assumed in order to study effective actuation parameters with stability analysis.

Glannopoulos et al (2007) [5] investigated a simple buckled beam with two full-length piezoelectric actuators; one was attached on the top and the other under the bottom of substrate. The energy method with inextensible constraint was employed to calculate snap-through voltages vs. end-displacements. Cazottes et al (2008) [6] did experiments using Macro Fiber Composite (MFC) as an extensional piezoelectric actuator attached on a clamped buckled beam and tested for snap-through voltages for various actuator's positions.

From the literature reviewed above, a majority of the research has paid attention to smart beams, which are midplane-symmetrically bonded with two full-length piezoelectric materials. There has been very little research reported on deformation characteristics of a smart beam with a segmented piezoelectric actuator attached on only one side, their influence on snap-through phenomenon and the relation of the critical electric field with the piezoelectric patch length. Consequently, in this study a buckled beam bonded with a segmented piezoelectric actuator is investigated. Simple-simple and clamped-clamped (encastré) support conditions are considered. The mathematical models are formulated from the energy method of inextensible beams. Deformed shapes and their associated stability for various end shortening distances and electric field strength are analyzed. Snap-through voltage for each case is computationally evaluated. Experiments are also conducted to validate the results obtained from the energy model developed. Optimum length of the segmented piezoelectric material that provide minimum snap-through voltage is determined for future applications.

2. Bistable smart beam

2.1 Beam components

The smart beam considered consists of a metal strip made of zinc-coated steel and a segmented piezoelectric patch bonded on a strip's planform surface at the central location as shown in Fig. 1. The metal strip acts as passive elastic substrate, whereas the piezoelectric patch functions as an actuator.

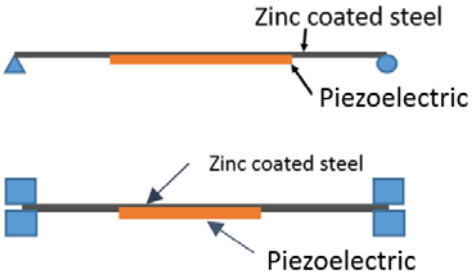

Fig. 1 The smart beam: (a) simply supported beam, (b) clamp-clamp supported beam.

2.2 Snap-through mechanism

The schematic sketching of snap-through buckling is illustrated in Fig. 2. Initially, the undeformed smart beam is compressed on the shorter edges until it is buckled into the fundamental buckling shape. Subjected to a specified end displacement, the buckled shape in Fig. 2 is considered to be in the 1st stable equilibrium position (configuration 1). When the piezoelectric material is electrically actuated with quasi-static positive voltage, the material is gradually expanded and an equivalent moment is induced to deform the beam (configuration 2). At a critical voltage, the beam becomes unstable (configuration 3) so it is displaced suddenly and snapped-though to the 2nd stable position (configuration 4).

3. Mathematical modeling

3.1 Smart beam geometry

The smart beam is assumed to be a slender thin walled structure so that the model can be treated as one dimensional and thus all kinematic variables are functions of the coordinate x as illustrated in Fig. 3. Also, it is hypothesized that the projected length of piezoelectric actuator attached on the buckled beam is approximately the same as the initial length s_0 although projected length of the substrate L is considered to be slightly smaller than its original dimension L_0 by the end displacement d_0 or $L = L_0 - d_0$.

Cross section of the smart beam at the central location can be seen as a laminate as shown in Fig. 4. The 1st and 2nd layers are the zinc coated steel substrate and piezoelectric material layer, respectively. In the figure h_k denotes thickness. Subscript k represents that the corresponding quantity belongs to the k^{th} layer.

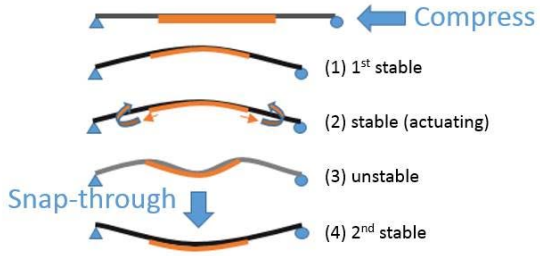

Fig. 2 Deformations of a bistable buckled beam

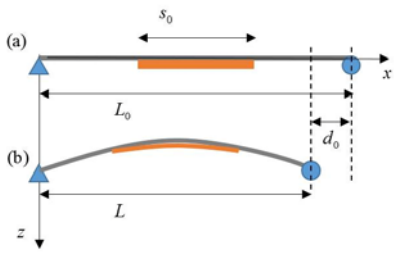

Fig. 3 dimensions of smart beams: (a) pre-compressed beam, (b) buckled beam

Fig. 4 Layers of a smart beam

3.2 Energy equations of buckled smart beam

The strain energy of each layer U_k can be written in Eq. (1). Subscript $k = 1$ is denoted for zing coated steel layer, while $k = 2$ is for piezoelectric layer.

$$U_1 = \frac{1}{2}\int_0^{h_1}\int_0^{L} E_1(\varepsilon_x)^2\, dx\, dz$$
$$U_2 = \frac{1}{2}\int_{h_1}^{h_1+h_2}\int_{\frac{L-s_0}{2}}^{\frac{L+s_0}{2}} E_2(\varepsilon_x - 2\varepsilon_V)\,\varepsilon_x dx\, dz \quad (1)$$

In the above, E_k is the extensional modulus in the x direction. ε_x is the total strain that obeys the Kirchhoff's hypothesis of a laminated beam [10] as expressed in Eq. (2). ε_V is free piezoelectric strain as shown in Eq. (3) [7].

$$\varepsilon_x = -z\frac{\partial^2 w}{\partial x^2} \quad (2)$$

$$\varepsilon_V = d_{11}\frac{V}{p} \quad (3)$$

where w denotes the beam deflection. d_{11} is the piezoelectric constant of the actuator. V is the applied voltage. p is the gap length between positive and negative electrodes.

The smart beam is assumed to be inextensionable during the deformation, so the constraint is derived from Eq. (4) and written compactly in Eq. (5).

$$L + d_0 = \int_0^L \left(1 + \left(\frac{dw}{dx}\right)^2\right)^{\frac{1}{2}} dx \approx \int_0^L \left(1 + \frac{1}{2}\left(\frac{dw}{dx}\right)^2\right) dx \quad (4)$$

$$g = L\left(d_0 - \frac{1}{2}\int_0^L \left(\frac{dw}{dx}\right)^2 dx\right) = 0 \quad (5)$$

The total potential energy Γ, which is the combination of strain energy U_k in Eq. (1) and the constraint g in Eq. (5) can be written as

$$\Gamma = \sum_{k=1}^{2} U_k + \lambda g = \Pi + \lambda g \quad (6)$$

In Eq. (6), λ is Lagrange's multiplier that represents the constraint force per unit area. In this formulation if the value of d_0 is considered to be positive, the positive Lagrange's multiplier signifies the compressive constraint force.

3.3 Ritz method

The solutions for the deflection $w(x)$ of the buckled smart beam can be approximated by using the Ritz method. The assumed functions is formed by using Hermitian formulations as written in Eqs. (7)-(8)

$$w(x) = \sum_{i=0}^{n}\left(d_i\psi_i^0(\mathrm{x}) + \theta_i\psi_i^1(\mathrm{x})\right) \quad (7)$$

$$\psi_i^0(\mathrm{x}) = \sum_{k=0}^{p} a_k (x)^k$$
$$\psi_i^1(\mathrm{x}) = \sum_{k=0}^{p} b_k (x)^k \quad (8)$$

where d_i is displacement coefficients, θ_i is slope coefficients, the i subscript represent node order located from left (0) to right (n) of beam structure. The domain between node i-1 and node i are designated as element number i. $\psi_i^0(x)$ and $\psi_i^1(x)$ are polynomial functions associated with displacement and slope coefficients, respectively and defined on the domain of elements i and i+1 that are adjacent to node i. a_k and b_k are function parameters, which can be determined by using Eq. (9).

$$\psi_i^0(\mathrm{x}_j) = \begin{cases} 1; i = j \\ 0; i \neq j \end{cases}, \quad \frac{d\psi_i^0(\mathrm{x}_j)}{dx} = \begin{cases} 0; i = j \\ 0; i \neq j \end{cases}$$
$$\psi_i^1(\mathrm{x}_j) = \begin{cases} 0; i = j \\ 0; i \neq j \end{cases}, \quad \frac{d\psi_i^1(\mathrm{x}_j)}{dx} = \begin{cases} 1; i = j \\ 0; i \neq j \end{cases} \quad (9)$$

Note that these function parameters have different values depending on how many elements of beams are divided and how many nodes are in each element. In the solution presentation in the next section, the notation "eX nY" will be employed to represent that over the beam length there are X elements, each of which has Y nodes. According to the Ritz method, these polynomial functions must be satisfied essential boundary conditions. For a simply supported beam the essential boundary conditions at both ends are $w(0) = w(L) = 0$ but for a clamped-clamped beam they are $w(0) = w(L) = w'(0) = w'(L) = 0$.

The equilibrium equations that are utilized to solve for d_i, θ_i and λ at any value of V can be obtained by finding the extremum of the total potential energy as indicated in Eq. (10).

$$\frac{\partial\Gamma}{\partial d_i} = 0, \quad \frac{\partial\Gamma}{\partial\theta_i} = 0, \quad \frac{\partial\Gamma}{\partial\lambda} = 0 \quad (10)$$

After all of the unknown coefficient is calculated. The critical electric field can be determined by analyzing the plots between the applied voltage versus Lagrange's multiplier. This will be discussed in more details in the following section.

3.4 Stability testing

Bordered Hessian matrix $\bar{H}_n$ expressed in Eq. (11) is utilized to test stability of the equilibrium shapes of the buckled smart beam.

$$\bar{H}_n = \begin{bmatrix} 0 & gd_1 & gd_2 & \cdots & gd_n & g\theta_1 & g\theta_2 & \cdots & g\theta_1 \\ gd_1 & \Pi dd_{11} & \Pi dd_{12} & \cdots & \Pi dd_{1n} & \Pi d\theta_{11} & \Pi d\theta_{12} & \cdots & \Pi d\theta_{1n} \\ gd_2 & \Pi dd_{21} & \Pi dd_{22} & \cdots & \Pi dd_{2n} & \Pi d\theta_{21} & \Pi d\theta_{22} & \cdots & \Pi d\theta_{2n} \\ \cdots & \cdots & \cdots & \cdots & \cdots & \cdots & \cdots & \cdots & \cdots \\ gd_n & \Pi dd_{n1} & \Pi dd_{n2} & \cdots & \Pi dd_{nn} & \Pi d\theta_{n1} & \Pi d\theta_{2n} & \cdots & \Pi d\theta_{2n} \\ g\theta_1 & \Pi \theta d_{11} & \Pi \theta d_{12} & \cdots & \Pi \theta d_{1n} & \Pi \theta\theta_{11} & \Pi \theta\theta_{12} & \cdots & \Pi \theta\theta_{1n} \\ g\theta_2 & \Pi \theta d_{21} & \Pi \theta d_{22} & \cdots & \Pi \theta d_{2n} & \Pi \theta\theta_{21} & \Pi \theta\theta_{22} & \cdots & \Pi \theta\theta_{2n} \\ \cdots & \cdots & \cdots & \cdots & \cdots & \cdots & \cdots & \cdots & \cdots \\ g\theta_n & \Pi \theta d_{n1} & \Pi \theta d_{n1} & \cdots & \Pi \theta d_{nn} & \Pi \theta\theta_{n1} & \Pi \theta\theta_{n2} & \cdots & \Pi \theta\theta_{nn} \end{bmatrix} \quad (11)$$

where $gd_i = \dfrac{\partial g}{\partial d_i}$, $g\theta_i = \dfrac{\partial g}{\partial \theta_i}$ for i = 1, 2, …, n and

$$\Pi dd_{ij} = \frac{\partial^2 \Pi}{\partial d_i \partial d_j}, \ \Pi d\theta_{ij} = \frac{\partial^2 \Pi}{\partial d_i \partial \theta_j}, \ \Pi \theta d_{ij} = \frac{\partial^2 \Pi}{\partial \theta_i \partial d_j},$$

$$\Pi \theta\theta_{ij} = \frac{\partial^2 \Pi}{\partial \theta_i \partial \theta_j} \text{ for } i, j = 1, 2, \ldots, n$$

Stability of each state can be identified with sign sequences of bordered leading principle minors from bordered Hessian matrix. If sign sequences are shown as $|\bar{H}_2|, |\bar{H}_3|, |\bar{H}_4|, \ldots, |\bar{H}_n| < 0$, then that state is a stable equilibrium, otherwise is an unstable equilibrium [8].

4. Computational Results

4.1 Characteristic of the buckled smart beam

The dimensions and material properties of the smart beam used in this sample calculation are tabulated in Tables. 1 and 2, respectively. The relations of the applied voltage V and Lagrange's multiplier λ are illustrated in Fig. 5. When $V = 0$ the smart beam is at the 1st stable buckled shape or configuration 1 with a positive Lagrange multiplier or compressive end force resulting from end-shortening. The corresponding deformed shape at this configuration is shown in Fig. 6, revealing small curvature at the middle part of the beam due to additional stiffness from the piezoelectric layer. When the smart beam is actuated with plus voltage ($V > 0$) in Fig. 5, the piezoelectric material is, therefore, elongated. Larger compressive reaction force from supports (higher λ) is induced during this electric field increment until the middle shape of the beam starts to be inverted from configuration 1 to 3. At this state, at λ = 290 N/m^2 the applied voltage reaches the limit point, or the critical voltage V_s. A slightly higher electric field input leads to a noncontinuous sudden change in shape or snap-through to configuration 4. The sudden transition during snap-though action results in the decreasing of λ such that it becomes a negative value, or equivalently the constraint force acting on the smart beam is in tension after snap-through. Subsequently, if the electric field is decreased, the smart beam gradually changes to configuration 5 until reaches the state of zero voltage at configuration 6. The inverted buckled shapes of the smart beam in configurations 4 – 6 with the decreasing electric field are also comparatively illustrated in Fig. 6. The stability checking is also performed by using Eq. 11.

Table. 1 Dimension of smart beam's component

Dimension (mm)	Piezoelectric actuator [9]	Zinc-coated steel
Thickness	0.3	0.2
Length	85	345

Table. 2 Properties

Properties	Piezoelectric actuator [9]	Zinc-coated steel
Young modulus, E (GPa)	30.34	78.427
Piezoelectric coefficient, d_{11} $(\frac{pC}{N})$	4.6x10^2	-

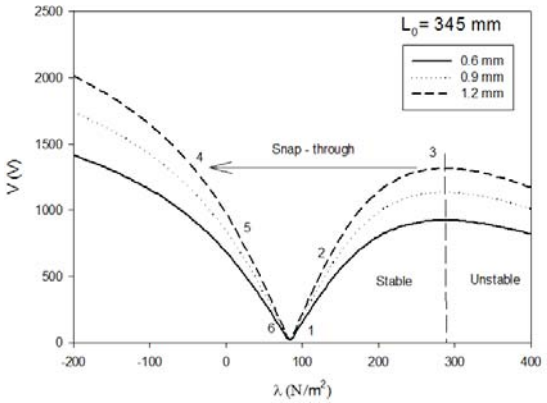

Fig. 5 Relations of applied voltage V and Lagrange's multiplier λ of end-displacements d_0 = 0.6, 0.9 and 1.2 mm

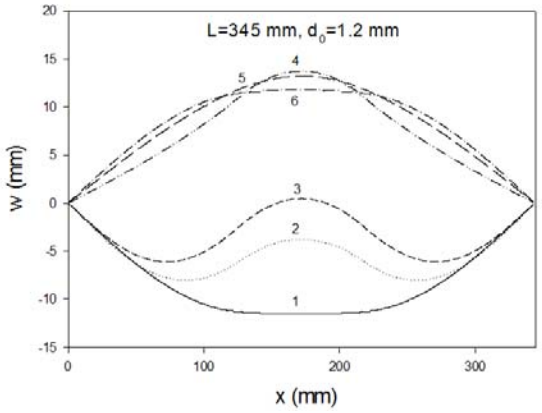

Fig. 6 Shape deformation for d_0 = 1.2 mm

The computation confirms the state of stable equilibrium of initial configuration 1 and moderately activated configuration 2. However, when the voltage reaches the critical value the beam turns into unstable equilibrium at configuration 3, and dynamically jumps to the other adjacent stable state, configuration 4. If the electrical field is reduced to zero, the beam follows the stable equilibrium configuration path 4 – 5 – 6 and finally attains the inactivated inverted shape.

In different perspective shown in Fig. 7, the relationship between mid-span displacement $w_{L/2}$ and V indicates the occurrence of the snap-through action at the 3rd configuration, which is a limit point of the buckled smart beam. The critical voltage V_s is approximately 1300 V in this case. It should be noted that there theoretically appears the other limit point in the figure if the negative voltage is applied to the smart beam in configuration 6. This negative field will cause the snap-back phenomenon, which can finally bring the smart beam back to its original shape in configuration 1.

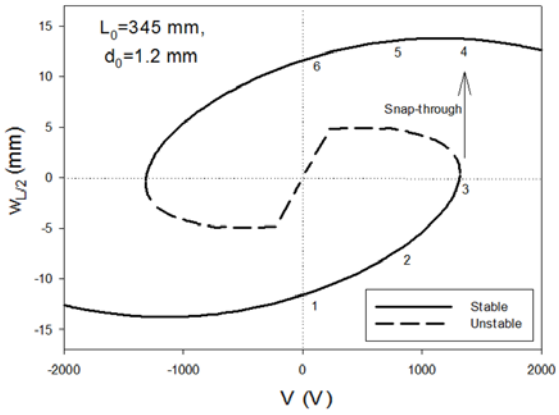

Fig. 7 Relation of mid-span displacement $w_{L/2}$ and applied voltage V

4.2 Optimum length of segmented actuator

It can be seen from the above results that a single segmented piezoelectric actuator bonded on the smart beam can be utilized to activate the snap-through motion. Thus, it is interesting to investigate and search for the most effective length s_0 of the segmented piezoelectric actuator that requires the lowest applied critical voltage. Non-dimensional variables, i.e. dimensionless actuator length $s_0^* = s_0/L_0$, dimensionless end-displacement $d_0^* = d_0/L_0$, and dimensionless critical electric field in term of equivalent free piezoelectric strain $\varepsilon_{V_s} = d_{33}V_s/p$ are formulated and used in the following parametric studies to enable extension of the particular computational results by similitude law.

Relations of ε_{V_s} versus s_0^* regarding the different values of d_0^* are plotted in Figs. 11 and 12. The figures show the optimum actuator length is about 60 percent of the total span length for the simply supported smart beam, and is approximately 50 percent of the substrate length in the case of encastré smart beam irrespective of how large the edge compression is. It is also seen that the dimensionless critical electric field is not a linear function of the end shortening distance. A softening effect on the flexural stiffness of the buckled smart beam is obviously perceived, since the increasing rate of snap-through voltage is significantly slower than that of the end displacement.

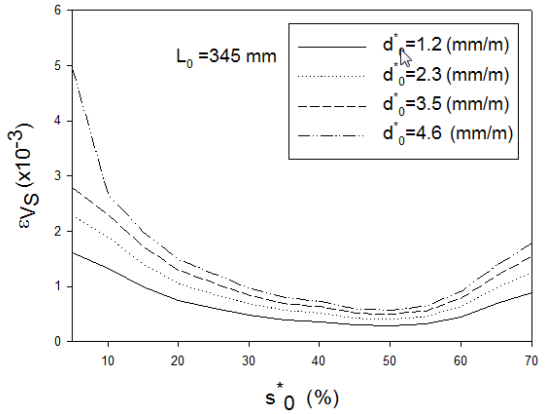

Fig. 8 Dimensionless voltage vs. end distance relations of simply supported buckled smart beams (Hermitian e3 n3)

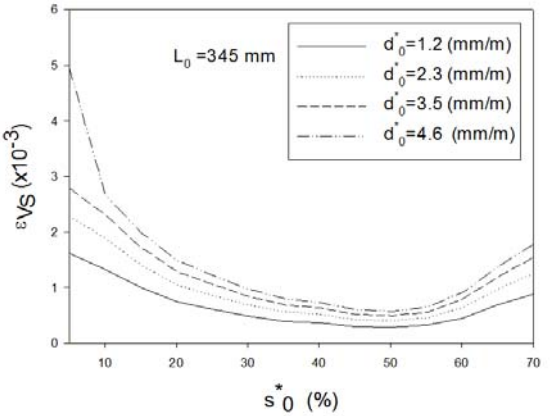

Fig. 9 Dimensionless voltage vs. end distance relations of encastré buckled smart beams (Hermitian e7 n2)

5. Model validation

This section presents some validation of V_s and initial amplitude of the buckled beam $w_{L/2}$ obtained from the present energy model with the experiment. The simply supported smart beam cases are chosen for validation. The details of experiment setup are described in the following subsections.

5.1 Experiment

A smart beam having the same dimensions and properties as used in the simulation is fabricated for the experiment. A Macro fiber composite (MFC) model 8528-P1 was adopted as the piezoelectric layer and it is adhered to the zinc-coated steel at the middle of the metal substrate by a thin layer of Loctite E20P epoxy glue. Conductive epoxy is utilized to connect the MFC electrodes with electrical wires. The photo of test specimen is shown in Fig. 9. It should be mentioned that the end mounting of the smart beam was meticulously designed to achieve simple support condition. Two aluminum rods are machined and longitudinally slotted with high precision in order to assemble to the beam with transition fit. The rods on the other hands were pulled to sit on the V-shaped support jig all the time by two small coil springs located at each end as shown in Figs. 10 and 11.

The schematic diagram of experiment setup is shown in Fig. 12. During the tests, the smart beam specimen was connected on grippers of a universal testing machine that can control the end-displacement d_0 parameter. The end displacement d_0 was varied from 0.3 to 1.6 mm. The voltage signal was generated by a computer and sent out through an A to D cards, Ni cDAQ-9172, a cards reader device that interchange signals between analog to digital from cards to a computer. After that, the signal was changed to analog by the Ni 9263 card. Then, the signal was fed to Piezo Driver, voltage amplifier, whose output was electrically wired to the MFC actuator and also send signal back to computer by the Ni 9215 card. Multimeter was also used for match the voltage between the MFC actuator and a computer. Before and after actuation, the residue voltage from the MFC was discharged by a resistor to neutralize the system.

In the experiment, the voltage amplitude was steadily increased and stopped immediately after the snap-through had detected. Each cases were repeated for 3 times and their mean values of data are presented. The voltage on a computer monitor was double checked with a multimeter. The voltage amplitude was controlled to stay in the range of 0 to 1400 volt in order to prevent the over-voltage supply to the MFC [9].

5.2 Validation results

The relationship between V_s and d_0 as well as the middle displacement before actuating $w_{0,L/2}$ and d_0 are illustrated in Fig. 13. The results show very good agreement between the present energy model and experiment. For the sake of comparison, Hermitian Ritz function e3 n3 and e7 n2 are also presented in the figure, from which slight discrepancies can be observed. This validation ensures the accuracy and applicability of the developed mathematical model.

Fig. 10 MFC actuator on a zinc-coated steel beam with simple support ends.

Fig. 11 Detail of simple support jig

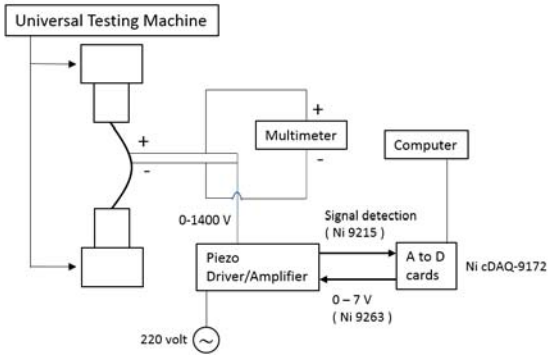

Fig. 12 Schematic diagram of experiment

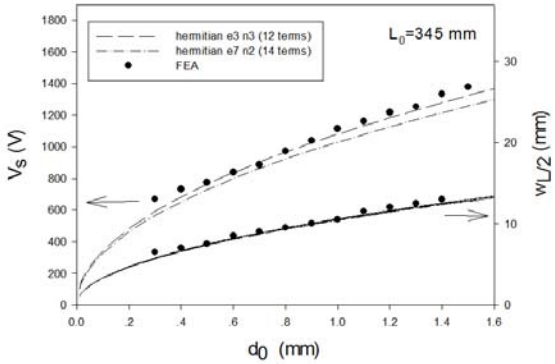

Fig. 13 Validated results of $w_{0,L/2}$ and V_s compare d_0

6. Conclusion

A mathematical models of piezoelectrically-induced snap-through buckling in a buckled beam bonded with a segmented piezoelectric actuator is developed. The computational results are validated with the experiments and excellent agreements can be found. The model can be used to predict snap-through voltages and the corresponding actuated shapes of buckled smart beams with different piezoelectric actuator sizes and various end shortening displacements. For simply supported buckled smart beams, the optimum actuator size is about 60 percent of the substrate length in order to the minimum critical voltage, whereas for encastré buckled smart beams, the optimum actuator size is approximately 50 percent of the substrate length. However, it should be noted that in this study, piezoelectric actuator is only placed symmetrically with respect to the middle location on a buckled beam. Therefore, further investigation should be performed to search for the possible global minimum snapping voltage in the case of an asymmetric segmented actuator.

7. Reference

[1] C. Paul et al. (2009). Bistable Buckled Beam: Modeling of Actuating Force and Experimental Validations, *Journal of Mechanical Design, ASME,* October 2009, Vol. 131.

[2] B. Camescasse et al. (2013). Bistable buckled beam: Elastica modeling and analysis of static actuation. *International Journal of Solids and Structures 50,* (2013) 2881-2893.

[3] B. Camescasse et al. (2014). Bistable buckled beam and force actuation: Experiment validations. *International Journal of Solids and Structures 51,* (2014) 1750-1757.

[4] C. Maurini et al. (2006). Distributed piezoelectric actuation of a bistable buckled beam. *European journal of mechanics A/Solids,* 26 (2006) 837-853.

[5] Georgios, G et al. (2007). Snap-through buckling behavior of piezoelectric bimorph beams: I. Analytical and numerical modeling. *Smart material and structures,* 2007, 16 pp. 1148-1157.

[6] P. Cazottes et al. (2008). Actuation of bistable buckled beams with Macro-Fiber Composites. Acropolis Convention Center, Nise, France. *International Conference on Intelligent Robots and Systems,* Sept, 22-26, 2008.

[7] A. Deraemaeker et al. *Mixing rules for the piezoelectric properties of Macro Fiber Composites (MFC),* URL:https://dipot.ulb.ac.be/dspace/bitstream/2013/62720/1/paper_v2.pdf, accessed on 10/6/2014.

[8] A. C. Chiang and K. Wain Wright. (2005). Fundamental Methods of Mathematical Economics, ISBN: 007-123823-9, McGraw Hill, United States of America.

[9] Smart Material Cooperation *MACRO FIBER COMPOSITE-MFC properties* URL**:** http://www.smart-material.com/MFC-product-main.html, accessed on 31/08/ 2013.

[10] M. W. Hyer (1997). Stress Analysis of Fiber-Reinforced Composite Materials, ISBN: 0-07-016700-1, WCB/Mc Graw-Hill, United States of America.